Authors' response – ACP

Radiative closure and cloud effects on the radiation budget based on satellite and ship-borne observations during the Arctic summer research cruise PS106
by Barrientos Velasco et al.

We thank the reviewers for the time and effort that they invested into the review of our manuscript, and for their helpful comments and suggestions. The description of the modifications considered in the manuscript can be found below. To address each point, we copied in red the last comment from the Referee and described our changes in black. Additionally, we added a screen-shot of the modified manuscript for some of the comments. In the screen-shots are marked in red the text that has been deleted and in blue the text that has been added in the latest version of the manuscript.

Comment 1

new comment: I didn't meant to have a detailed explication/equation on how the adiabatic liquid water content is calculated. Lines 170- 178 are not needed (but thanks for clarifying!). Just mentioning that the liquid water content profile is assumed to be an adiabatic profile is fine. Are you scaling the profile with the LWP of the MWR? This information could be added after the sentence in line 167.

What is not clear to me is how reff can be calculated by Frisch et al (2002) in case of mixed-phase clouds. Since Z is dominated by the ice you do not have a Z for the liquid cloud droplets only. Please comment and also add further information in the manuscript.

Response: Lines 170-178 were deleted from the manuscript. It was also specified that the profile was scaled with the LWP that comes from the MWR in line 167.

Regarding the calculation of reff, we agree that the reflectivity which is used to calculate the liquid droplet effective radius might be influenced by ice crystals. During PS106, most liquid droplets in mixed-phase clouds were observed in clouds with cloud top temperatures >-10°C (see Figure below). Bühl et al. (2016) showed that for mixed-phase clouds with cloud top temperatures >-10°C the reflectivity at heights were likely only ice crystals were present was usually below -40dBZ (see Fig. 7 in Bühl et al. (2016)). During PS106, the vast majority of the cloud radar reflectivity at the heights where liquid layers were observed in mixed-phase clouds was around -20dBZ. Therefore, we are confident that the reflectivity, which was used to derive the cloud droplet effective radius, was actually dominated by the liquid cloud droplets rather than ice crystals. To avoid an influence of the ice crystals on the reflectivity, which is used to derive the cloud droplet effective radius, a cloud radar Doppler peak separation, as e.g. proposed by Kalesse et al. (2019) and Radenz et al. (2019), would be necessary. These techniques are, however, not yet operational.

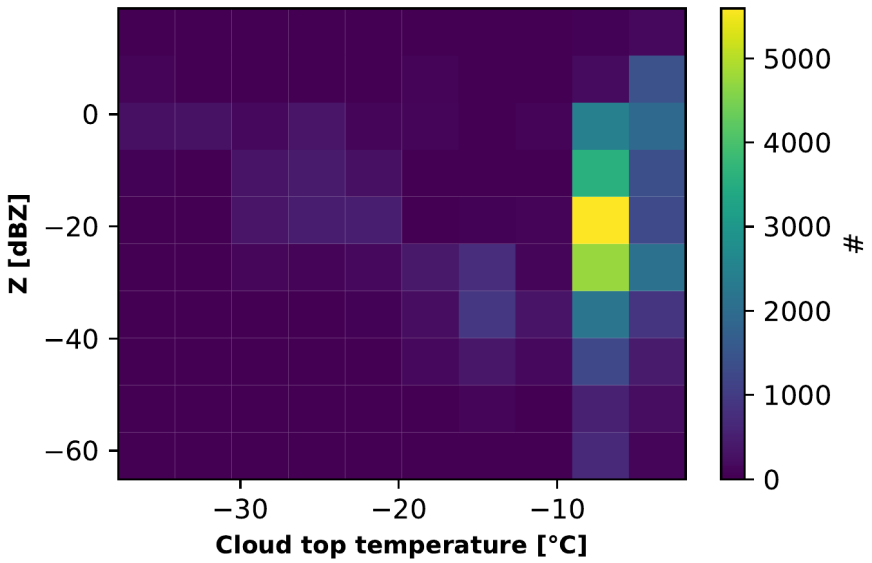

Figure 1. 2D histogram depicting the frequency of occurrence of the radar reflectivity factor [dBZ]at different cloud top temperature [°C] for mixed-phase cloud cases during PS106.

Additional information has been added to the manuscript regarding the derivation of liquid effective radius as seen below.

Once a cloudy pixel is identified, the cloud water content and effective radius are determined regardless if the cloud is detected as a single or mixed-phase cloud. The liquid water path is retrieved based on the HATPRO MWR measurements using the retrieval method developed in Löhnert and Crewell (2003). This method relies on a long-term radiosonde training data set, which in this case is based on Ny-Ålesund, NO (78.9°N, 11.85°E, WMO Code 6260). Once Q_L is known, the liquid water content (q_L) and $r_{E,L}$ are determined. The $r_{E,L}$considers the radar reflectivity factor and measurements of the integrated cloud liquid water based on the methodology described in Frisch et al. (2002). The retrieval of q_L is obtained by distributing the observed the Q_L from the HATPRO MWR adiabatically among the identified liquid and mixed-phase cloud pixels classified by the Cloudnet algorithm. This method assumes a log-normal cloud-droplet size distribution, which is constant with height. The uncertainties of q_L are calculated by error propagation assuming a typical uncertainty of 20-25 gm^{-2} in Q_L (Löhnert and Crewell, 2003). The adiabatic increase of liquid water is based on Brenguier (1991) and calculated by the following equation in .

$$\frac{dq_L}{dz} = -\left(1-\left(\frac{C_p \cdot T}{L \cdot e}\right)\right) \cdot \left(\frac{1}{\left(\frac{C_p \cdot T}{L \cdot e}\right)+\left(\frac{L \cdot qs \cdot \rho a}{p-es}\right)}\right) \cdot (\rho a \cdot g \cdot e \cdot es) \cdot (p-es)^{-2}.$$

In Eq. **??**, T is the atmospheric temperature in , p is atmospheric pressure in , qs is the specific humidity mixing ratio in , es is the saturated vapour pressure, ρa is the density of air in (see Eq. **??**), e is the ratio of the molecular weight of water vapour of dry air equal to 0.62198, g is retrieval of $r_{E,L}$ considers the radar reflectivity factor and the profile of Q_L based on the acceleration due to gravity -9.81 , C_p is the heat capacity of air at a constant pressure 1005.0 , L is methodology described in Frisch et al. (2002). The reflectivity used to derive the $r_{E,L}$ was likely not affected by the presence of ice crystals since most of the mixed-phase cloud cases observed during PS106 had cloud top temperatures larger than -10 °C and a radar reflectivity around -20 dBZ (not shown). The study of Bühl et al. (2016) showed that at these temperatures and radar reflectivities, the latent heat of evaporation 2.5×10^6 , R_d is the specific gas constant for dry air 287.04 signal of the mixed-phase cloud is dominated by the presence of liquid droplets rather than the ice crystals. In cases where the radar reflectivity is lower (e.g., -40 dBZ) the ice crystals dominate more the signal of the mixed-phase cloud and other methods are necessary to derive the $r_{E,L}$ (Kalesse et al., 2019; Radenz et al., 2019).

Comment 2

new comment: Please expicitely mention in the manuscript what you did with the cloud properties, e.g. averaged 2 bins vertically and linear interpolation in time. You just mention which grid you use in the RTM but not how you adjust the cloud properties accordingly.

Response: The text has been edited as follows in Section 2.3:

2.3 Radiative transfer simulations

The TROPOS Cloud and Aerosol Radiative effect Simulator (henceforward T-CARS) is a Python-based framework to carry out radiative transfer simulations with a particular focus on the investigation of the radiative effects of aerosols and clouds. Parts of this framework have already been applied and described in Barlakas et al. (2020) and Witthuhn et al. (2021). T-CARS enables the use of various sources for input data such as atmospheric profiles of trace gases, temperature, humidity, properties of clouds, aerosols, and surface parameters. The present study employs the widely used rapid radiative transfer model (RRTM) for GCM applications (RRTMG; Mlawer et al. (1997); Barker et al. (2003); Clough et al. (2005)).

In this study, the daily T-CARS output files have a standard grid that consists of 197 atmospheric levels ranging from the surface up to 20 km height and with km height and 1-minute temporal resolution. The first 10 km km of the atmosphere is divided into 160 levels with a geometric layer thickness of 62.5 m. The m. The level thickness of each pixel for the first 10 km of the atmosphere corresponds to two vertical levels of Cloudnet's pixel which are averaged to the standard grid. The following 5 km km of the atmosphere have a layer thickness of 250 mm, while the last 5 km km of the atmosphere a layer thickness of 193.8 mm.

Comment 3

new comment: I am sorry. This question was misleading. What I was hinting at: single-layer clouds can be devided into liquid, ice, mixed-phase. Why is there another category precipitation for single-layer clouds? To me it is not clear why single-layer clouds which are precipitating can not be classified as well.

In the figure caption you mention "mixed-phase clouds of type 1 or 2" but only the first one is shown.

Response: The reason to have the precipitation category is to treat those cases with extra caution. The cloud products and flux observations can have larger uncertainties under precipitation events. This has been clarified in the paper with the following text:

The cloud phase flag was included to analyse the thermodynamic phase of clouds. Even though it is available for the entire PS106 time series, the focus is here directed to the thermodynamic phase of single-layer clouds , since these cases are the most frequent, and an analysis is less complex than for multilayer conditions. Fig. 5b Figure 5b shows on only single-layer cloud periods. This figure indicates an occurrence frequency of 32.6 36.7 % for single-layer mixed-phase clouds of type two (ice and super-cooled droplets), 16.8 19.4 % for mixed-phase clouds of type one (well-separated ice and liquid phase), and 15.6 21.5 % for single layer ice clouds. The remaining period is composed of single-layer clouds with precipitation (13.6 17.9 %), clear-sky periods (12.1 %), and single layer liquid clouds (2.7 4.5 %). We emphasise the need to consider precipitation periods since, during these events, there are larger uncertainties in observations (i.e., cloud radar, lidar, MWR, and radiometers).

We apologize since the wrong figure was accidentally chosen when compiling the manuscript. The label of Figure 5 has been corrected.

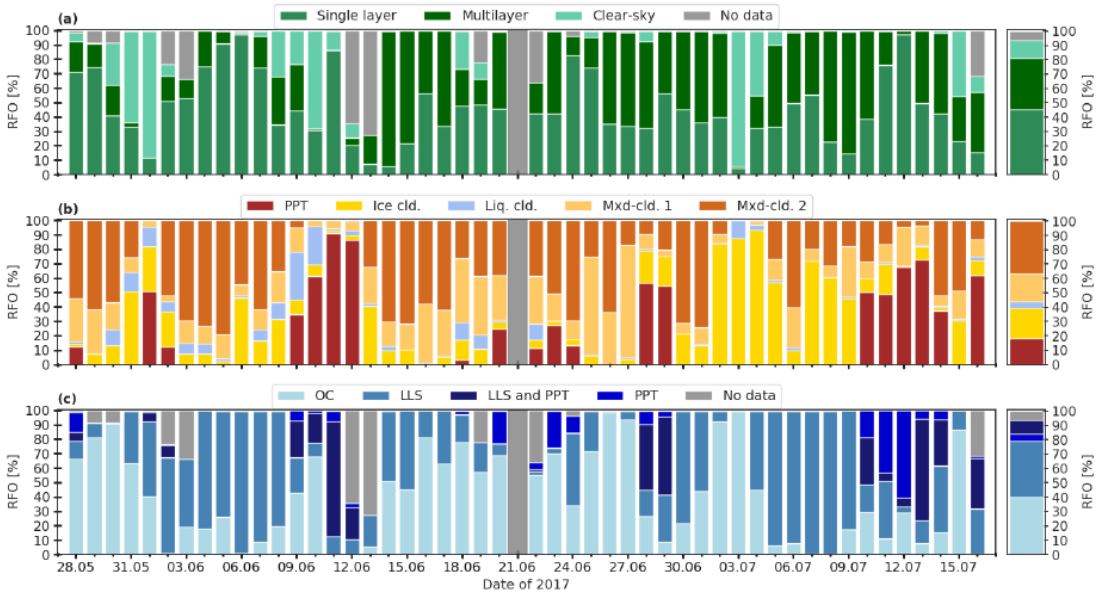

Figure 5. Daily and overall relative frequency of occurrence (RFO) of various cloud characteristics. Panel (a) shows the RFO of clear-sky, single-level clouds, and multilayer clouds. Panel (b) shows the RFO of the thermodynamic phase of single-layer clouds, differentiating periods of ice clouds, liquid clouds, mixed-phase clouds of type 1 or 2, and precipitation (PPT). Panel (c) is the RFO of various quality flags indicating optimum conditions (OC), low-level stratus (LLS), PPT and simultaneous occurrence of LLS and PPT.

Comment 4

new comment: I would have liked to seen a least a short critical discussion in the manuscript about how realistic these assumptions on the uncertainties in the input parameters are and which uncertainties might be there in addition which have not been considered. As I mentioned, there are other uncertainties (using hourly model data not capturing the full temporal variability of water vapor and temperature, the assumption of Ts=T10m,…) I think that it is really important to remind the reader of those ones as well.

Response: We agree that neglecting aerosols, extrapolating hourly data to 1 minute resolution, assuming near-surface temperature as skin temperature, and using model data for water vapour and temperature atmospheric profiles can lead to additional uncertainties. We emphasised these points even further with the following text in the manuscript (section 3.2).

‘It is worth clarifying that additional uncertainties come from neglecting the presence of aerosols, the assumption of near-surface temperature as skin temperature, the extrapolation of hourly data into 1-min resolution, the assumption that the spatial interpolation from 0.25° latitude by 0.25° longitude (i.e., ERA5 data set) or 1° latitude by 1° longitude (i.e., CERES SYN1deg products) can capture the atmospheric and surface conditions and variability experienced during PS106. While it was attempted to quantify some of these uncertainties, a careful and more specific analysis should be extended in a different experimental setup.’

It is worth clarifying that additional uncertainties come from neglecting the presence of aerosols, the assumption of near-surface temperature as skin temperature, the extrapolation of hourly data to 1-min resolution, the assumption that the coarse spatial grid from 0.25° latitude by 0.25° longitude (i.e., ERA5 data set) or 1° latitude by 1° longitude (i.e., CERES SYN1deg products) can capture the atmospheric and surface conditions and variability experienced during PS106. While it was attempted to quantify some of these uncertainties (e.g., the omission of aerosols in Fig. B1 and section 3.4.1), a careful and more specific analysis will be made by carrying out several sensitivity analyses to quantify these uncertainties considering the observations from the Multidisciplinary drifting Observatory for the Study of Arctic Climate (MOSAiC) expedition (Shupe et al., 2022). Our primary focus will be on the spatiotemporal differences among shipborne, reanalysis and satellite observations, which we believe are the largest source of uncertainties.

3.3 Case studies

Comment 5

new comment: I think that this information, i.e. the further analyses you did to better understand the bias (i.e. varying input, testing with radiosonde,...) and the conclusion that the pyrgeometer measurements are likely influenced e.g. by the shipborne instrumentaion are of high relevance. This should definitely be included in more detail in the manuscript and in particular when you present and discuss the results of Fig.12. Just mentioning it as a aside in the conclusion points 2 and 3 is not sufficient.

Response: We agree with the comment. We have edited the following text in Section 3.4.1.

'Several simulations were conducted using only the Vaisala RS92-SGP radiosondes launched every 6 hours from *Polarstern* (Schmithüsen, 2017a, b), and a (Schmithüsen, 2017a, b), and also sensitivity analyses were made by varying the atmospheric temperature and humidity to try to match the observations of the LWD flux (not shown). However, the negative bias found for both T-CARS and CERES SYN1deg fluxes might also be caused by a positive bias of the ship-borne pyrgeometer observations, e.g., due to the influence of the exhaust plume of *Polarstern* or nearby instrumentation causing a fluctuation of temperature nearby the pyrgeometer. As there was only one pyrgeometer measurement aboard *Polarstern*, it is impossible to further investigate this hypothesis. However, for future campaigns, it is recommended here to operate two pyrgeometers installed in different locations of the research vessel to exclude such influences.'

The Several simulations were conducted using only the Vaisala RS92-SGP radiosondes launched every 6 hours from *Polarstern* (Schmithüsen, 2017a, b), and also sensitivity analyses were made by varying the atmospheric temperature and humidity to try to match the observations of the LWD flux (not shown). However, the negative bias found for both T-CARS and CERES SYN1deg fluxes might also be caused by a positive bias of the ship-borne pyrgeometer observations, e.g., due to the influence of the exhaust plume of *Polarstern* or other factors affecting the pyrgeometer. As there was only one pyrgeometer measurement aboard *Polarstern*, it is impossible to further investigate this hypothesisbias. However, for future campaigns, it is recommended here to operate two pyrgeometers installed in different locations of the research vessel to exclude such influences.

Comment 6

new comment: The reason for this second peak should also be included in the manuscript, i.e. when discussing of Fig. 12.

Response: We agree with this point. Bellow is presented the additional description to the second peak. Additionally, is shown the difference between the previous version of the paper and the current one.

'The second peak centred around -50.0 Wm^{-2} in Fig. 12d is most likely due to momentary obstructions on the observations that were not captured by the initial screening that affected about 5 data points of CERES SYN1deg simulations. It is also possible that part of the bias might be due to the presence of aerosols. However, since the behaviour for pristine and clear-sky conditions is similar, this cause is not the leading the bias for the second peak. In general, the biases of both T-CARS and CERES SYN1deg are both within the uncertainty limit of ±20 Wm^{-2} indicating that radiative closure is determined for both data sets.'

The comparison for the SWD flux uses a stricter screening of data, which also excludes all periods when the pyranometer's field of view was obstructed by the superstructure of *Polarstern*. For T-CARS, a positive bias of 44.2 $\mathrm{W\,m^{-2}}$ and a correlation coefficient of 0.85 were found initially without this screening. With screening, a bias of 9.5 $\mathrm{W\,m^{-2}}$ and a correlation coefficient of 0.95 were obtained. In the case of CERES SYN1deg, the biases for all-sky, clear-sky, and pristine conditions were found to have values of -27.1 $\mathrm{W\,m^{-2}}$, 3.6 $\mathrm{W\,m^{-2}}$, and 12.0 $\mathrm{W\,m^{-2}}$, respectively. These values confirm that the larger negative bias for all-sky conditions is due to the presence of clouds that were captured within the CERES SYN1deg footprint but did not pass over the shipborne remote sensing instrumentation. The second peak centred around -50.0 $\mathrm{W\,m^{-2}}$ in Fig. 12d is most likely due to momentary obstructions on the observations that were not captured by the initial screening that contains about 5 data points of CERES SYN1deg simulations. In general, the biases of both T-CARS and CERES SYN1deg are both within the uncertainty limit of ± 20 $\mathrm{W\,m^{-2}}$ indicating that radiative closure is achieved determined for both data sets.